

JET PHYSICS AT HERA

HANS-CHRISTIAN SCHULTZ-COULON

*Universität Dortmund, 44221 Dortmund, Germany**

Jet production in electron-proton collisions at HERA provides a unique testing ground for Quantum Chromodynamics (QCD). Apart from the determination of the strong coupling constant α_s , ep jet data may especially be used to gain insight into the dynamics of the exchanged parton cascade, whose structure is probed by the high- E_T dijet system; thus information on the parton content of the proton and (quasi-)real and virtual photons is obtained. This report touches some of these aspects revealed in recent jet data from the HERA experiments which are testing perturbative QCD at the limits of applicability.

1 Introduction

Multi-jet production in deep inelastic ep -scattering (DIS) provides special sensitivity to the mechanisms of the strong interaction and can hence be used to test the predictions of perturbative Quantum Chromodynamics (pQCD) in a rather inimitable way. This is especially true since the HERA experiments deliver data over a large range of both the four-momentum transfer, Q^2 , of the exchanged photon and the transverse energy of the observed jets, E_T .

In lowest order, multi-jet production in DIS is described by the QCD-Compton and the boson-gluon fusion processes (Figure 1), with the momentum distributions of the incoming partons taking part in the hard interaction given by the parton density functions (PDFs) of the proton; the Q^2 -evolution of the latter is described by the DGLAP equations¹ which in lowest order are equivalent to the assumption of exchanging a strongly k_t -ordered parton cascade, k_t being the transverse momentum of the partons within the cascade. However, as illustrated by the generic diagram in Figure 1c, to calculate ep jet cross sections requires additional terms, such that in certain parts of phase space, where k_t -ordered parton emission is no longer manifest, the standard DGLAP approach has to be extended e.g. with the concept of photon structure, which preserves the perturbative ansatz of the DGLAP evolution scheme but results in an artificial violation of the k_t -ordering. Within this concept, high E_T jets can be produced not only by direct processes in which the virtual photon interacts as a point-like particle with a parton out of the proton, but also by resolved processes where the photon interacts hadronically. In the photoproduction limit ($Q^2 \rightarrow 0$), the cross section is thus sensitive to the

*This work was supported by the BMBF, contract no. 7D055P.

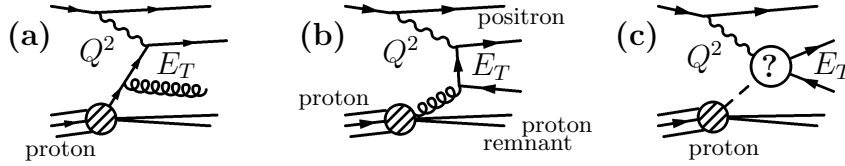


Figure 1. Schematic Feynman diagrams for the dijet production mechanism with (a) the QCD-Compton and (b) the boson-gluon fusion process; (c) generic picture for dijet production via photon-parton fusion where the actual interaction mechanism is unknown and to be resolved by the dijet system. The two scales involved in these processes are indicated as the four-momentum transfer Q^2 and the transverse jet energy E_T .

parton distributions of both the photon and the proton at a scale set by the transverse energy of the jets, E_T .

The two scales involved in ep jet production, $\sqrt{Q^2}$ and E_T , can now be used to resolve the structure of the photon-parton interaction in general. Several kinematic regions can be distinguished, depending on the absolute and relative sizes of these two scales. In the regime where Q^2 and E_T^2 are both large, perturbative methods are clearly justified and the DGLAP ansatz can be used to extract information on the proton structure and the strong coupling α_s . Typically, leading-order (LO) Monte Carlo models approximate higher order pQCD contributions in this regime by parton showers. If $Q^2 \ll E_T^2$ the jet cross sections become sensitive to the hadronic structure of the photon. The region where $Q^2 \approx E_T^2$ is of special interest, since in this regime the DGLAP ansatz is expected to break down for small values of the variable x_B (Bjorken- x) revealing effects of non- k_t -ordered parton cascades. Characteristics expected from other evolution schemes like BFKL² or CCFM³ could be observable in this phase space regime.

Any deviations from next-to-leading order (NLO) predictions may, however, simply indicate that fixed order calculations beyond NLO are needed. These may also help to resolve other ambiguities associated with high E_T jet production in DIS: where Q^2 and E_T^2 both are substantially large ($\gg \Lambda_{QCD}^2$) there is ambiguity in the choice of the renormalization scale^a. It is important to know where these ambiguities have a significant effect on the cross sections.

2 Testing pQCD at Large Scales

Jet production at large Q^2 and large E_T has been studied by both the H1 and the ZEUS collaborations. In this regime the choice of the renormaliza-

^aAnalogously such ambiguity exists also for the factorization scale. However, since the effects due to the choice of the renormalization scale are generally larger, this ambiguity is not explicitly mentioned in the context of this paper.

tion scale ($\mu_r = \sqrt{Q^2}$, E_T) is of minor importance since scale dependencies of the cross sections are generally small if μ_r is large. Hence NLO order calculations are expected to provide a good description of the data as can be seen from Figure 2 which shows the inclusive jet cross section $d^2\sigma/dE_T dQ^2$ measured by H1⁴. Jets have been defined using the inclusive k_\perp algorithm⁵ in the Breit frame where the photon collides head-on with the incoming proton. Over the whole analyzed phase space the DISENT NLO calculation⁶, using the CTEQ5M1 PDFs as input⁷ and corrected for hadronization effects ($< 10\%$), agrees perfectly well with the data. The size of the scale uncertainties together with the error contribution from hadronization corrections can be inferred from Figure 2 (right). From these data, H1 extracts the strong coupling constant α_s in bins of E_T , chosen to be the renormalization scale. The QCD predictions are fitted to the jet cross sections using the CTEQ5M1 parameterization of the PDFs and the strong coupling constant as the single free parameter. The result is shown in Figure 3 and clearly indicates the running of α_s according to the renormalization group equation. A combined fit to all 16 data points shown in Figure 2 results in

$$\alpha_s(M_Z) = 0.1186 \pm 0.0030 \text{ (exp.)}_{-0.0045}^{+0.0039} \text{ (theo.)}_{-0.0023}^{+0.0033} \text{ (pdf)} \quad (\mu_r = E_T),$$

where the largest contributions to the experimental error come from uncertainties of the hadronic energy scale. The theoretical error is dominated by

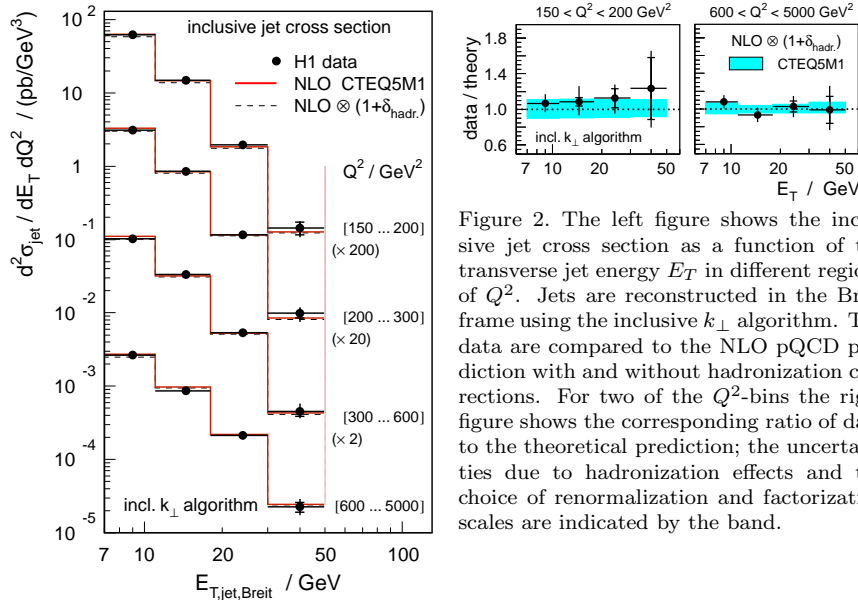


Figure 2. The left figure shows the inclusive jet cross section as a function of the transverse jet energy E_T in different regions of Q^2 . Jets are reconstructed in the Breit frame using the inclusive k_\perp algorithm. The data are compared to the NLO pQCD prediction with and without hadronization corrections. For two of the Q^2 -bins the right figure shows the corresponding ratio of data to the theoretical prediction; the uncertainties due to hadronization effects and the choice of renormalization and factorization scales are indicated by the band.

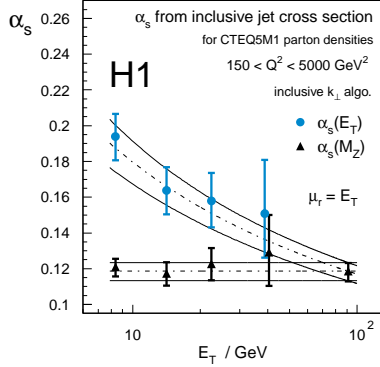
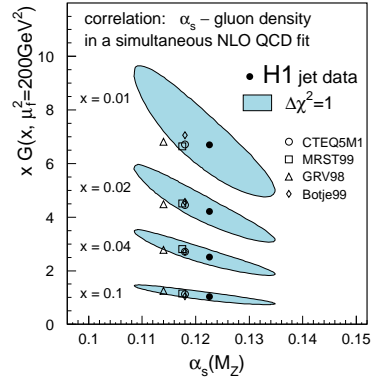


Figure 3. Determination of α_s from the inclusive jet cross section for the renormalization scale $\mu_r = E_T$. The results are shown for each E_T value (circles) including experimental and theoretical uncertainties. The single values are extrapolated to the Z^0 -mass (triangles). The final result $\alpha_s(M_Z)$ (rightmost triangle) is obtained in a combined fit. The curves represent the combined result and its uncertainties once at the Z^0 -mass (lower curves) and once evolved according to the renormalization group equation (upper curves).

Figure 4. The correlation of α_s and the gluon density in the proton from a fit to H1 jet and inclusive DIS data for different values of the fractional momentum x of the gluon. The central fit result is indicated by the full marker while the error ellipses show the experimental and theoretical uncertainties.



the uncertainty in the hadronization corrections and the dependence on the choice of the renormalization scale. The uncertainty in the knowledge of the parton density functions has been estimated⁴ using the correlated errors provided by a recent QCD analysis⁸ together with its global PDF-fits. This error contribution is substantially reduced when using the dijet rate R_{2+1} to extract α_s as done by the ZEUS collaboration⁹, leading to the preliminary result

$$\alpha_s(M_Z) = 0.1166^{+0.0039}_{-0.0047}(\text{exp.})^{+0.0055}_{-0.0042}(\text{theo.})^{+0.0012}_{-0.0011}(\text{pdf}) \quad (\mu_r = \sqrt{Q^2}).$$

Both measurements of α_s depend on the knowledge of the parton content of the proton. Vice versa, by using the best knowledge on α_s one can use (multi-)jet cross section measurements to extract the quark and gluon densities in the proton⁴. A test of pQCD independent of data from other experiments, has been made by the H1 collaboration⁴ in performing a simultaneous determination of both quantities. This is done in a fit to the inclusive jet and dijet cross sections together with the inclusive DIS cross section, where the latter is restricted to the kinematic range $150 \leq Q^2 \leq 1000 \text{ GeV}^2$ and only constrains the quark densities in the proton. The results of this fit are shown in Figure 4 as a correlation plot between $\alpha_s(M_Z)$ and the gluon density $xg(x)$ evaluated at four different values of the gluon momentum fraction $x = 0.01$,

0.02, 0.04 and 0.1. While the present data do not allow a simultaneous determination of both parameters with competitive precision the sensitivity to the product $\alpha_s \cdot xg(x)$ can clearly be seen.

3 Scale Ambiguities

The relevance of the choice of the renormalization scale at smaller Q^2 can be seen from Figure 5, showing the dijet cross section as a function of $\log Q^2$ as measured by the ZEUS collaboration¹⁰. As for the inclusive jet cross section, pQCD in NLO describes the data down to values of $Q^2 \approx 150 \text{ GeV}^2$. However, at Q^2 values below 150 GeV^2 scale uncertainties become large and the choice of the renormalization scale is no longer irrelevant: while NLO calculations using $\mu_r = \sqrt{Q^2}$ describe the dijet cross section down to $Q^2 \approx 10 \text{ GeV}^2$, this is no longer the case for $\mu_r = E_T$.

This issue has also been studied by the H1 collaboration¹¹ investigating dijet event rates, R_2 , at low values of the Bjorken- x variable $10^{-4} < x_B < 10^{-2}$ and low Q^2 , $5 < Q^2 < 100 \text{ GeV}^2$. For different requirements on the transverse energies $E_{T,(1,2)}$ of the final state jets, NLO QCD calculations are confronted with the data using two different choices of the renormalization scale $\mu_r = \sqrt{Q^2}$ and $\mu_r = \sqrt{Q^2 + E_T^2}$. Figure 6 summarizes the preliminary result of this analysis in two representative (x_B, Q^2) -bins. At large Q^2 ($Q^2 = 71 \text{ GeV}^2$) and large x_B ($x_B = 4.7 \cdot 10^{-3}$) the theoretical calculation is

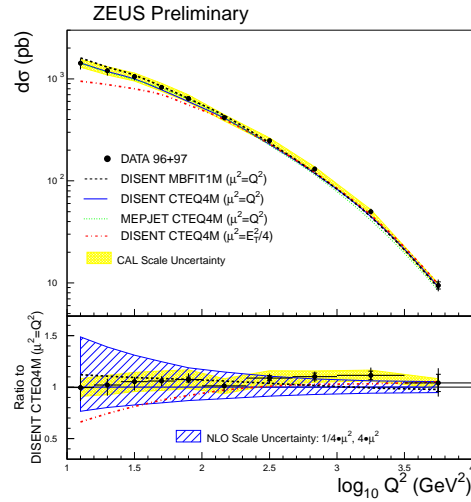


Figure 5. (a) The dijet cross section $d\sigma/d\log Q^2$ for jets in the Breit frame using the inclusive k_\perp algorithm. The points represent the data with statistical (inner bars) and total (outer error bars) uncertainties. The shaded band indicates the systematic uncertainty due to the energy scale of the ZEUS calorimeter. While the theoretical predictions using $\mu_r = \sqrt{Q^2}$ describe the measured cross section rather well, the dashed-dotted line representing a NLO calculation with $\mu_r = \sum E_{T,i}/2$, where $E_{T,i}$ are the transverse jet energies of the jets, falls below the data for $Q^2 < 150 \text{ GeV}^2$. This can also be seen from (b) which shows the ratio of the measured cross section to the NLO prediction using CTEQ4M PDFs and $\mu_r = \sqrt{Q^2}$.

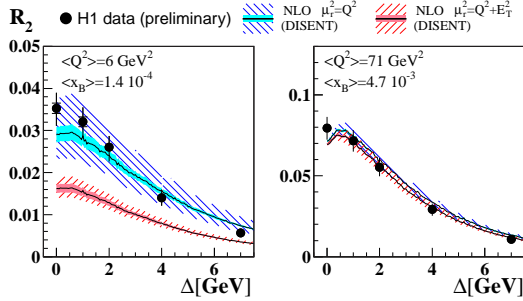


Figure 6. Dijet rate R_2 at two values of x_B , Q^2 as a function of the transverse energy requirement $E_{T,1} > (5 + \Delta)$ GeV on the jet with larger E_T ; for the second jet the transverse energy $E_{T,2}$ must be above 5 GeV.

rather insensitive to the choice of the scale (Fig. 6, right), and — in agreement with the results from the dijet cross section measurement at high Q^2 — gives a good description of the data^b. In contrast, one obtains no safe theoretical prediction at low x_B , Q^2 (Fig. 6, left): although data and NLO QCD calculation do agree for $\mu_r = \sqrt{Q^2}$, the large scale uncertainties lead to almost vanishing predictive power of the theory; choosing, however, a larger scale $\mu_r = \sqrt{Q^2 + E_T^2}$ such that scale uncertainties become small, leads to clear disagreement between the measured event rate R_2 and the next-to-leading order QCD calculation, independent of the requirement on the transverse energy of the jets $E_{T,1} > (5 + \Delta)$ GeV. This indicates the necessity to include higher-order contributions by introducing, for example, the concept of photon structure. Choosing the same scale $\mu_r = \sqrt{Q^2 + E_T^2}$, comparison of the data with the NLO calculations by JetViP¹³ including a resolved photon contribution, indeed shows better, although not perfect agreement¹¹.

4 Probing Parton Dynamics

In order to further investigate the interplay of the two scales $\sqrt{Q^2}$ and E_T , the ZEUS collaboration has studied¹⁴ the cross section for jets produced at large pseudo rapidities as a function of the ratio E_T^2/Q^2 . When compared to LO Monte Carlo models (Figure 7) the data are well described for $E_T^2 \ll Q^2$. However, only those models which include non- k_t -ordered parton emission (ARIADNE¹⁵, RAPGAP¹⁶) reproduce the $E_T^2/Q^2 \approx 1$ region; the full range can be described solely by models which include a resolved photon contribution as the RAPGAP Monte Carlo and a NLO calculation by JetViP. A

^bThis is true unless a symmetric transverse energy cut is applied where the NLO QCD calculation becomes infrared sensitive¹². In this region resummed calculations are needed but not yet available. Thus the presented measurement also provides an important reference for improved theoretical predictions.

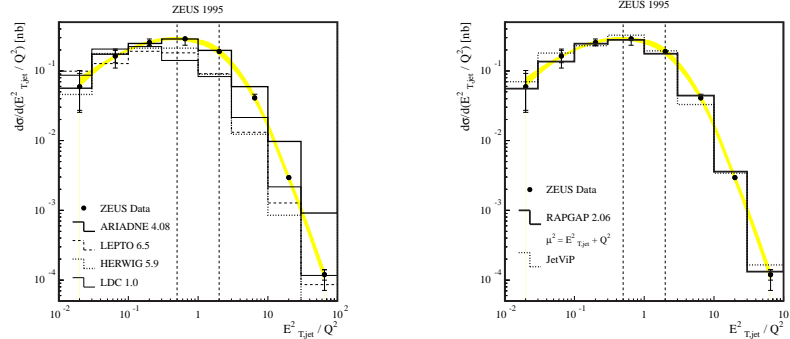


Figure 7. Forward-jet cross section as a function of E_T^2/Q^2 in comparison (a) to several LO Monte Carlo predictions and (b) to RAPGAP and a NLO JetViP calculation both including resolved photon contributions. The shaded band corresponds to the energy scale uncertainty of the ZEUS calorimeter.

reasonable description of these data is also found in a recent comparison¹⁷ with Monte Carlo predictions based on the CCFM³ evolution equation which, by means of angular-ordered parton emission, is equivalent to the BFKL² approach for $x \rightarrow 0$ while reproducing the DGLAP equations at large x .

To explore a possible signature of BFKL dynamics, the $Q^2 \approx E_T^2$ regime has been analyzed in more detail studying the x_B -dependence of forward particle production^c. Figure 8 shows the x_B -dependence of the forward-jet and forward- π^0 cross sections in this region^{14,18} in comparison to Monte Carlo models with and without a resolved photon contribution and — in case of the π^0 cross sections — a LO BFKL calculation. The need for an additional contribution to the direct γp -interaction can clearly be seen from these figures as the data are rather well described by models including a resolved photon component. Moreover, the π^0 measurement, which accesses very small polar angles, is actually best described by a BFKL-based leading-order calculation¹⁹ when taking hadronization corrections into account. However, large theoretical scale uncertainties diminish the significance of these comparisons.

5 Jets in Photoproduction

The production of hard dijet events in photoproduction is dominated by resolved photon processes in which a parton in the photon with momentum fraction x_γ is scattered from a parton in the proton. Hence studies of dijet production can be used to investigate the hadronic structure of the photon

^cParticles produced at very small polar angles w.r.t. the incoming proton direction.

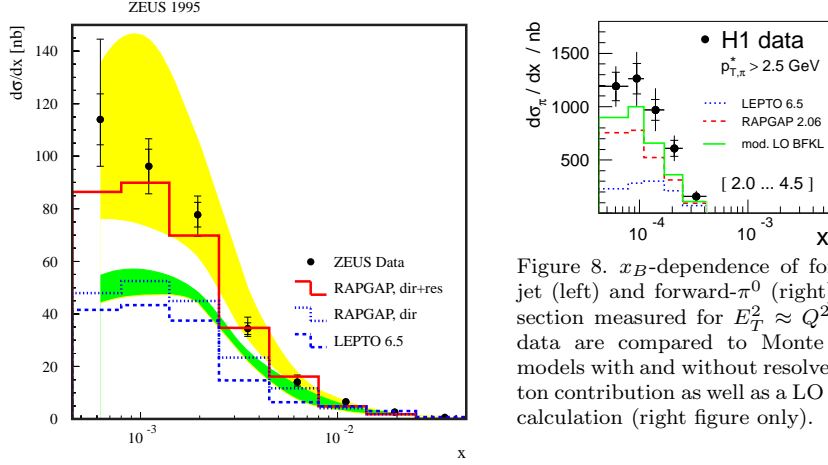


Figure 8. x_B -dependence of forward-jet (left) and forward- π^0 (right) cross section measured for $E_T^2 \approx Q^2$. The data are compared to Monte Carlo models with and without resolved photon contribution as well as a LO BFKL calculation (right figure only).

at $Q^2 \approx 0$. In leading order the cross section is proportional to the photon flux $f_{\gamma/e}$ and maybe approximated by use of effective parton densities for the proton and photon such that $\sigma_{dijet} \sim f_{\gamma/e} \cdot f_{\text{eff},\gamma} f_{\text{eff},p} \cdot |\mathcal{M}|^2$, where \mathcal{M} is the matrix element of the hard parton-parton scattering process and $f_{\text{eff},[\gamma,p]} = f_{q/[\gamma,p]} + f_{\bar{q}/[\gamma,p]} + 9/4 f_{g/[\gamma,p]}$. With this relation H1 extracts the gluon density of the photon²⁰ in leading order pQCD using the knowledge of $f_{\text{eff},p}$ from DIS and $f_{[q,\bar{q}]/\gamma}$ from the photon structure function F_2^γ as measured in e^+e^- collisions²¹. The result is shown in Figure 9 indicating a strong rise towards low x_γ .

The determination of the gluon content of the photon is however strongly affected by non-perturbative effects and the treatment of background from soft underlying events²⁰; it therefore can only be done using Monte Carlo programs which include phenomenological models to account for these effects but up to now are still restricted to leading order matrix elements. Other dijet analyses from H1²² and ZEUS²³ suppress these non-perturbative effects by harder E_T requirements for the jets and thus investigate the parton distributions in the photon at high x_γ ($x_\gamma \gtrsim 0.2$) where quark contributions dominate^d. A comparison of the NLO prediction with the dijet cross section measured by ZEUS²³ for $E_{T,jet} > 14$ GeV as a function of the pseudo rapidities of the two most energetic jets, η_1^{jet} and η_2^{jet} , is given in Figure 10. While the NLO calculation describes the data at large $x_\gamma \geq 0.75$ rather well,

^d Actually the dependence on $x_\gamma^{\text{obs}} = [E_{T,1} e^{-\eta_1^{\text{jet}}} + E_{T,2} e^{-\eta_2^{\text{jet}}}] / 2yE_e$ is studied, where E_e is the electron beam energy. In the leading order massless approximation x_γ^{obs} is equivalent to x_γ .

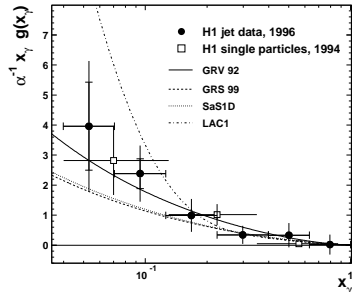


Figure 9. The gluon distribution of the photon multiplied by $\alpha^{-1}x_\gamma$ as a function of x_γ at a mean scale of $E_T^2 = 74 \text{ GeV}^2$.

a clear discrepancy is seen for the full x_γ -range if both jets are going in the forward direction (positive η^{jet}). This is where substantial contributions from resolved processes ($x_\gamma < 0.75$) are expected suggesting that, in the kinematic region of the measurement presented, the available parameterizations of the parton density functions of the photon are insufficient²³.

6 Conclusion

Measurements of ep jet production rates have been presented in a wide range of the four-momentum transfer Q^2 and the transverse jet energy E_T to study the dynamics of the underlying partonic interaction. At large scales $\mu_r = \sqrt{Q^2}$, E_T the data are successfully described by perturbative QCD allowing a determination of the strong coupling constant α_s and the gluon density in the proton. Scale ambiguities have been studied and, as Q^2 gets smaller, sensitivity of the NLO predictions to the choice of the renormalization scale is observed. At low Q^2 insight into the structure of the photon and effects of non- k_t -ordered parton evolution is revealed.

References

1. V.N. Gribov, L.N. Lipatov, Sov. J. Nucl. Phys. **15** (1972) 438, 675; Y.L. Dokshitzer, Sov. Phys. JETP **46** (1977) 641; G. Alterelli, G. Parisi, Nucl. Phys. **B126** (1977) 297.
2. E.A. Kuraev, L.N. Lipatov, V. Fadin, Soviet Phys. JETP **45** (1977) 199; Y.Y. Balitsky, L.N. Lipatov, Soviet J. Nucl. Phys. **28** (1978) 822; L.N. Lipatov, Soviet J. Nucl. Phys. **63** (1980) 904.
3. M. Ciafaloni, Nucl. Phys. **B296** (1988) 49; S. Catani, F. Fiorini, G. Marchesini, Phys. Lett. **B234** (1990) 339; Nucl. Phys. **B336** (1990) 18.
4. H1 Collab., DESY-00-145, submitted to Eur. Phys. J. C.

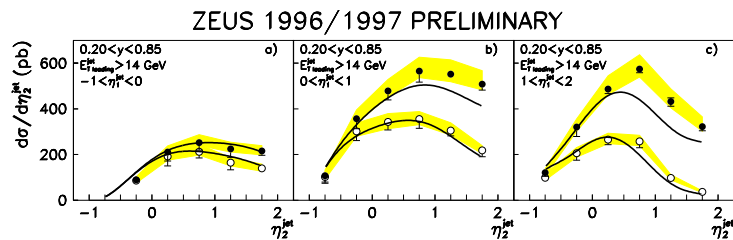


Figure 10. The dijet cross section for $E_{T,jet} > 14$ GeV as a function of η_2^{jet} in bins of η_1^{jet} . The solid data points correspond to the entire x_γ^{obs} range while the measurement for $x_\gamma^{obs} > 0.75$ is shown by the open points. The curves correspond to the NLO predictions and the shaded bands indicate the uncertainties related to the energy scale.

5. S.D. Ellis, D.E. Soper, Phys. Rev. **D48** (1993) 3160; S. Catani, Y.L. Dokshitzer, M.H. Seymour, B.R. Webber, Nucl. Phys. **B406** (1993) 187.
6. S. Catani, M.H. Seymour, Nucl. Phys. **B485** (1997) 291; Erratum-ibid. **B510** (1997) 503.
7. H.L. Lai et.al. Eur. Phys. J **C12** (2000) 375.
8. M. Botje, Eur. Phys. J **C14** (2000) 285.
9. ZEUS Collab., “Measurement of differential cross sections for dijet production in neutral current DIS at high Q^2 and a determination of α_s ”, ICHEP 2000, Osaka, Japan, July 2000.
10. ZEUS Collab., “A measurement of the dijet production cross section in neutral current deep inelastic scattering at HERA”, ICHEP 2000, Osaka, Japan, July 2000.
11. H1 Collab., “A measurement of dijet rates in deep inelastic scattering at HERA”, ICHEP 2000, Osaka, Japan, July 2000.
12. S. Frixione, G. Ridolfi, Nucl. Phys. **B507** (1997) 315.
13. B. Pötter, Comp. Phys. Comm. **119** (1999) 45.
14. ZEUS Collab., Phys. Lett. **B479** (2000) 1.
15. L. Lönnblad, Comp. Phys. Comm. **71** (1992) 15.
16. H. Jung, Comp. Phys. Comm. **86** (1995) 147.
17. H. Jung, G. P. Salam, CERN-TH-2000-318.
18. H1 Collab., Phys. Lett. **B462** (1999) 440.
19. J. Kwieciński, A.D. Martin, P.J. Sutton, Phys. Rev. **D46** (1992) 921.
20. H1 Collab., Phys. Lett. **B483** (2000) 36.
21. For a recent review see R. Nisius, Phys. Rept. **332** (2000) 165.
22. H1 Collab., Eur. Phys. J. **C13** (2000) 397; Eur. Phys. J. **C1** (1998) 97.
23. ZEUS Collab., “Measurement of dijet photoproduction at high transverse energies at HERA”, ICHEP 2000, Osaka, Japan, July 2000.